Scripta Materialia 180 (2020) 66–70

Contents lists available at ScienceDirect

Scripta Materialia

journal homepage: www.elsevier.com/locate/scriptamat

Refinement of the grain structure of additive manufactured titanium alloys via epitaxial recrystallization enabled by rapid heat treatment

Zhiyi Zou[a], Marco Simonelli[a,*], Juliano Katrib[b], Georgios Dimitrakis[c], Richard Hague[a]

[a] Centre for Additive Manufacturing, University of Nottingham, Nottingham NG8 1BB, UK
[b] Advanced Materials Research Group, University of Nottingham, Nottingham NG8 1BB, UK
[c] George Green Institute for Electromagnetics Research Group, Nottingham NG8 1BB, UK

ARTICLE INFO

Article history:
Received 15 November 2019
Revised 20 January 2020
Accepted 20 January 2020

Keywords:
Additive manufacturing
Titanium alloys
Epitaxial recrystallization
Rapid heat treatment

ABSTRACT

The coarse prior-β grain structure in titanium alloys produced by additive manufacturing is associated to mechanical anisotropy and limited fatigue life. Here we report a novel methodology to refine such structure by rapid heat treatment of Ti–6Al–4V produced by laser powder-bed fusion. The refinement was analysed using high-temperature EBSD that showed, for the first time, how high angle boundary β grains nucleated and grew with quasi-equiaxed morphology by epitaxial recrystallization. These findings show the potential for such heating regime to be applied to control grain size, morphology and distribution in a wider category of structural alloys produced by additive manufacturing.

© 2020 Acta Materialia Inc. Published by Elsevier Ltd.
This is an open access article under the CC BY-NC-ND license.
(http://creativecommons.org/licenses/by-nc-nd/4.0/)

Thanks to a combination of high specific strength, corrosion resistance and biocompatibility, titanium alloys – especially Ti–6Al–4V – have found a wide use in different applications [1–3]. One of the most promising manufacturing techniques for Ti–6Al–4V is laser powder-bed fusion (L-PBF), an attractive Additive Manufacturing (AM) technique that allows the production of net-shape components of complex geometry with minimal material waste [4]. Compared to wrought counterparts, Ti–6Al–4V components produced by L-PBF generally possess higher strength, though with an anisotropic behaviour alongside significantly lower ductility [2]. This is due to the typical microstructure of L-PBF Ti–6Al–4V consisting of martensitic α'-lamellae within coarse columnar prior-β grains, which might extend to hundreds of microns or even several millimetres along the building direction.

Previous investigations have shown that the martensitic α' structure of L-PBF Ti–6Al–4V can be decomposed into $\alpha+\beta$ by heat treatments conducted *below* the β transus temperature. The resulting microstructure generates a good balance of strength and ductility compared to the as-printed condition [2,5]. However, heat treatments below the β-transus temperature cannot change the original elongation of the prior-β grains and therefore have no impact on anisotropy and fracture toughness, thus limiting the use of such components. Studies on the microstructural evolution upon heat treatments *above* the β-transus temperature have shown that it is possible to obtain coarse equiaxed β grains; however, the extensive β grain growth associated with such heat treatments lead to an unacceptable loss in strength and ductility [6].

The principal aim of the present study is to investigate how the initial microstructure formed in L-PBF can be exploited to achieve β-grain refinement via Rapid Heat Treatment (RHT) methods. The recrystallization phenomena responsible for refinement and the mechanical properties following such RHT are discussed.

The materials used in this study were Ti–6Al–4V (grade 23) cylinders of 9 mm diameter and 60 mm length produced by L-PBF at 90° build angle to the build platform. The produced cylinders were manufactured on an EOSINT M290. Prior to RHT the average β-transus temperature of the specimens was estimated to be ~950 °C as ascertained by Simultaneous Differential Analysis (SDT). Five cylinders were subjected to the RHT protocol in an argon protective atmosphere using a bespoke setup that included an induction power supply with an operating frequency of 200 KHz and a maximum power level of 1 kW. This experimental set up enabled full β-annealing with a constant heating rate of 10 °C/s to a target temperature of 1030 °C and a short dwell time of 1 s before air cooling. Tensile specimens with a diameter of 4 mm and gauge length of 20.4 mm were machined from the centre of the cylinders according to standard ASTM E8/E8M-16a [7]. Tensile tests were conducted at room temperature (20 °C) on an Instron 5969 at a strain rate of 0.14 mm/min. Microstructural observations were carried out on representative samples before and after RHT using a JEOL 7100F FEG-SEM equipped with a heating SEM stage (Murano in-situ stages, Gatan) for a controlled

* Corresponding author.
E-mail address: marco.simonelli@nottingham.ac.uk (M. Simonelli).

https://doi.org/10.1016/j.scriptamat.2020.01.027
1359-6462/© 2020 Acta Materialia Inc. Published by Elsevier Ltd. This is an open access article under the CC BY-NC-ND license.
(http://creativecommons.org/licenses/by-nc-nd/4.0/)

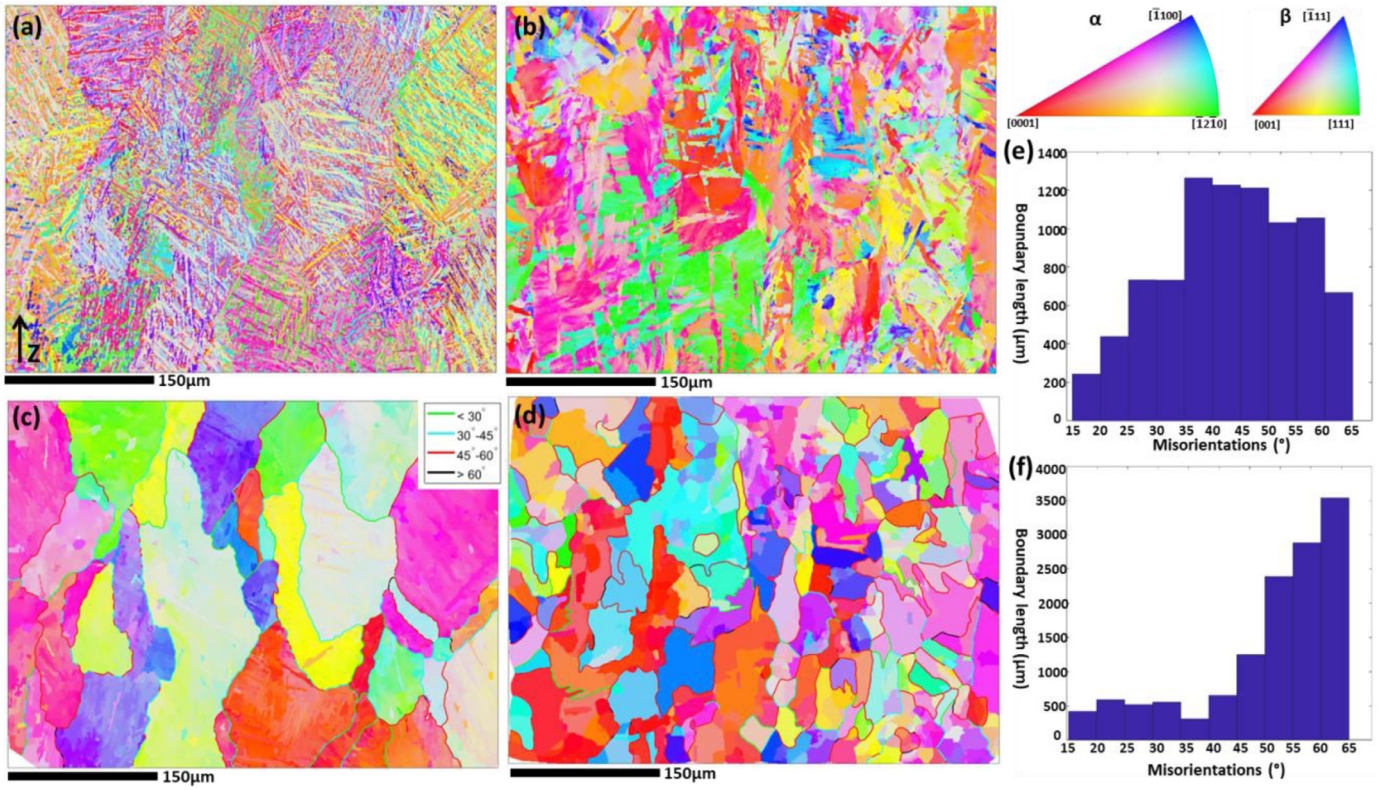

Fig. 1. Typical α-orientation maps of Ti–6Al–4V in (a) as-built condition and (b) after the proposed rapid heat treatment, both of the orientation maps were scanned with a step size of 0.5 μm. Reconstructed β-orientation maps from the as-built (c) and rapidly heat treated (d) microstructures. The misorientation distribution at the prior-β grain boundary in the as-built condition and after RHT are shown in (e) and (f), respectively. High angle boundaries are also colour marked in the reconstructed β-orientations maps.

heating of specimens (up to 980 °C) and simultaneous imaging and Electron Back-Scattered Diffraction (EBSD). The collected data was analysed using HKL-Channel 5^{TM}, OIM and the MATLAB toolbox MTex, mapping in Z-IPF with colour scheme presented in Fig. 1. If not directly measured at high-tempearture, the β-phase was reconstructed by back-calculation from the room temperature α-phase via the Burger Orientation Relationship (BOR) as described elsewhere [8]. Using this approach, each reconstructed β grain derived from a minimum of 4 different α variants.

The typical microstructure of the specimens in the as-built condition is shown in Fig. 1a. This consists of martensitic α' laths in coarse columnar β grains as commonly reported in the literature [2,8]. After RHT the microstructure develops a conventional $\alpha+\beta$ laminar structure with an increase in the α colony size (Fig. 1b). Most importantly it is observed a significant refinement of the β-grains which has never been reported before in AM specimens after heat treatment. This is confirmed in the orientation maps of the β phase (Fig. 1c and d) calculated from the room temperature microstructure in both conditions which show that the original elongated coarse morphology of the prior-β grains is substantially refined after RHT. The typical microstructure of the α phase in the as-built condition and after RHT is presented in the Supplementary material (Fig. S1). The comparison of the calculated β grain boundary angles reveals that after RHT there is an increase in high angle boundaries (HABs) as shown in Fig. 1e and f and marked via red and black boundaries in the orientation maps of Fig. 1c and d. This indicates that recrystallization of β might have occurred within the initial coarse columnar β grains during RHT.

The current understanding associated to the nucleation and growth of the β phase during conventional heat treatment of martensitic Ti–6Al–4V is that, after an initial recovery of the microstructure, the $\alpha+\beta\rightarrow\beta$ transition occurs by movement of the α/β interface until only the parent β phase exists [9,10]. It is also believed that nucleation of β grains of new orientations does not take place because the shear stress associated to the HCP $\rightarrow$ BCC lattice transformation is too low to induce recrystallization of β grains with no BOR with existing α during the $\alpha+\beta\rightarrow\beta$ transformation [9,10]. However, this would not explain the observed recrystallization and refinement of the β grains.

To understand the observed early stage refinement mechanisms, high-temperature EBSD was undertaken. This technique enabled the direct measurement of the orientations of the grain structure at elevated temperatures with sub-micron resolution. Fig. 2a and b show α- and β-orientation maps acquired at 850 °C where the orientation relationship in the two phases is expressed in the corresponding pole figures of Fig. 2c–f. The average orientations of marked grains in Fig. 2a and b are listed in Table 1. The orientation maps show the existence of multiple α variants contained in two distinct prior-β grains (Fig. 2a). Typically, there are 5–7 variants that are formed inside each prior-β grain (α_1-α_7). Within each prior-β grain the dominant β (for sake of clarity this is defined hereafter as β_1) is similarly orientated across the length of the entire prior-β grain (orientation spread $<10°$). As shown in Fig. 2c the $(0001)_\alpha$ plane of each α lath is parallel to one of the $(110)_\beta$ planes of β_1 and one to three $\langle 11\bar{2}0\rangle_\alpha$ reflections are parallel to one of the $\langle 111\rangle_\beta$, indicating that the β_1 is the parent phase that is strictly related to the martensitic phase via BOR.

However there are other (HAB) β grains that are distinct from the dominant β_1 as marked in Fig. 2b. It is observed that the β of new orientations can nucleate either on the grain boundary of the α (this will be referred as β_2) or on the grain boundary of the prior-β (hereafter indicated as β_3 and β_4). The analysis shows

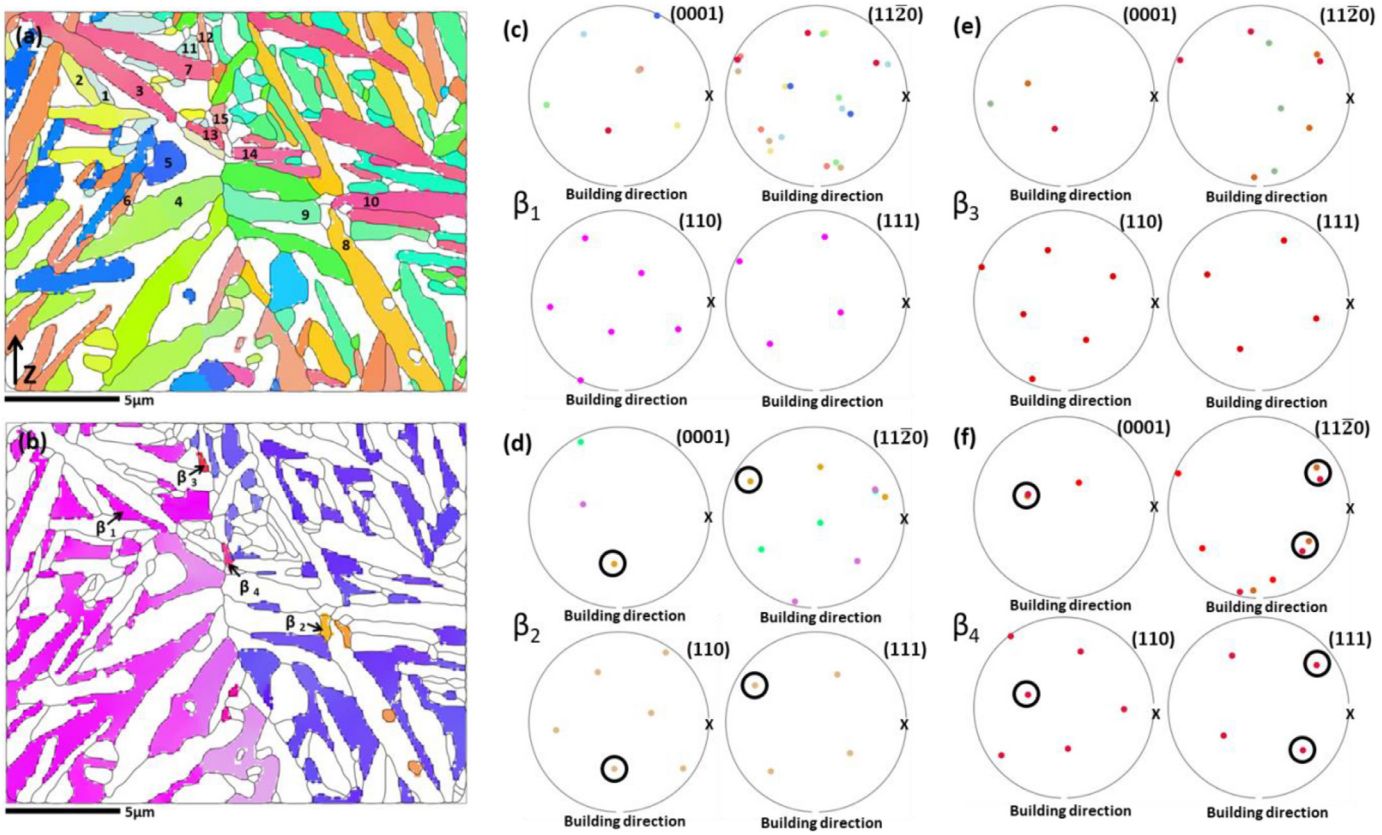

Fig. 2. α-orientation (a) and β-orientation (b) maps acquired at 850 °C, a step size of 0.14 μm was used to obtain the orientation data. The discrete pole figures in (c) show the orientation relationship between the parent β phase (indicated as β_1) and a cluster of nearby α laths. (d), (e) and (f) are discrete pole figures that show the orientation relationship of recrystallized β with neighboring α laths, black circles are used to highlighting BOR relationship. Colours refer to IPF-scheme demonstrated in Fig. 1.

Table 1
Average orientation of marked grains in Fig. 2a and b.

ID	Orientation
α1	(150°, 112°, 194°)
α2	(117°, 61°, 235°)
α3	(38°, 31°, 198°)
α4	(83°, 110°, 236°)
α5	(25°, 88°, 205°)
α6	(37°, 29°, 188°)
α7	(16°, 149°, 200°)
α8	(6°, 137°, 239°)
α9	(153°, 97°, 183°)
α10	(110°, 145°, 219°)
α11	(84°, 109°, 227°)
α12	(109°, 145°, 229°)
α13	(31°, 26°, 201°)
α14	(110°, 145°, 219°)
α15	(107°, 145°, 226°)
β1	(118°, 150°, 226°)
β2	(94°, 165°, 194°)
β3	(215°, 173°, 238°)
β4	(240°, 166°, 232°)

Table 2
Misorientations of β_2 and β_4 to surrounding dominant β.

	Grain	Misorientation (aixs/angle)
Surrounding dominant β (183°, 134°, 223°)	β2	[−1, 1, 1]/60.00°
	β4	[−1, 0, 1]/60.00°

that β_2 and β_4 are crystallographically related to individual adjacent α/α' laths via BOR (Fig. 2d–f). Both β_2 and β_4 have a ~60° misorientation with the surrounding dominant β (β_1). Such misorientation is not random but related to β_1 by precise axis-angle rotation pairs (Table 2). Therefore β_2 and β_4 appear to be nuclei of epitaxially recrystallized β, which is similar to that recently discovered in hot-worked metastable β titanium alloy [1]. These subgrains originate at the α/β interface and correspond effectively to one of the six equivalent BOR transformations that link the α to β phases. In addition, it is observed that there is another HAB β that does not show any apparent orientation relationship with adjacent α laths (β_3). The misorientation of β_3 relative to β_1 (or any of the other measured HAB β) is not described by any obvious axis-angle rotation pair (Fig. 2e). However, it cannot be excluded that β_3 originates from similar recrystallization mechanisms originating under the plane of investigation, as it will be discussed later.

The recrystallization phenomena that lead to the formation of HAB β are significantly different from the recovery of the $\alpha+\beta$ microstructure and the grain growth of the parent β phase (β_1) [2,10] and, to the authors knowledge, have never been reported before in any Ti alloys produced by any AM process. Drawing an analogy with the recrystallization of deformed Ti alloys, it is can assumed that the driving force for the observed epitaxial recrystallization derives from the stored energy of deformation that is typically expressed by the large dislocation densities found after L-PBF in the core and at the boundary of the martensitic as-built microstructure. The substructure of the martensitic α' could therefore seed epitaxial recrystallization of the β allowing for the formation of new β variants during the $\alpha+\beta\rightarrow\beta$ transformation. Previous research indicates that under similar heating rates of ~10 °C/s, there is only a marginal increase in the temperature of the onset $\alpha\rightarrow\beta$ transformation [10] and therefore the high-temperature EBSD (near equilibrium conditions) experiments presented in this study can capture the range of temperatures at which the phase trans-

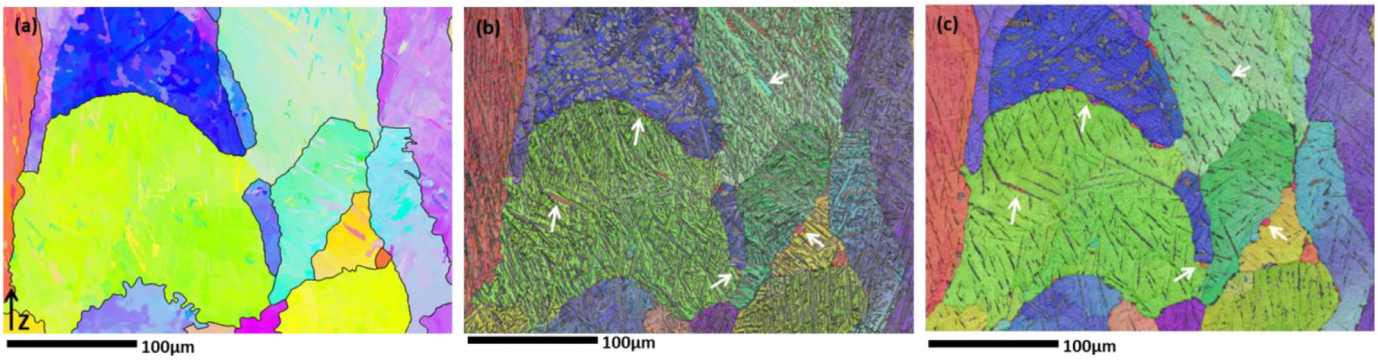

Fig. 3. (a) Reconstructed β-orientation map of specimen from the as-built condition, orientation data was acquired via a step size of 0.25 μm; (b) measured β-orientation maps of the same locations at 850 °C, the orientation data was measured by high-temperature EBSD with a step size of 0.25 μm; (c) measured β-orientation maps of the same locations at 925 °C, the orientation data was obtained via a step size of 0.6 μm. White arrows indicate recrystallized β grains.

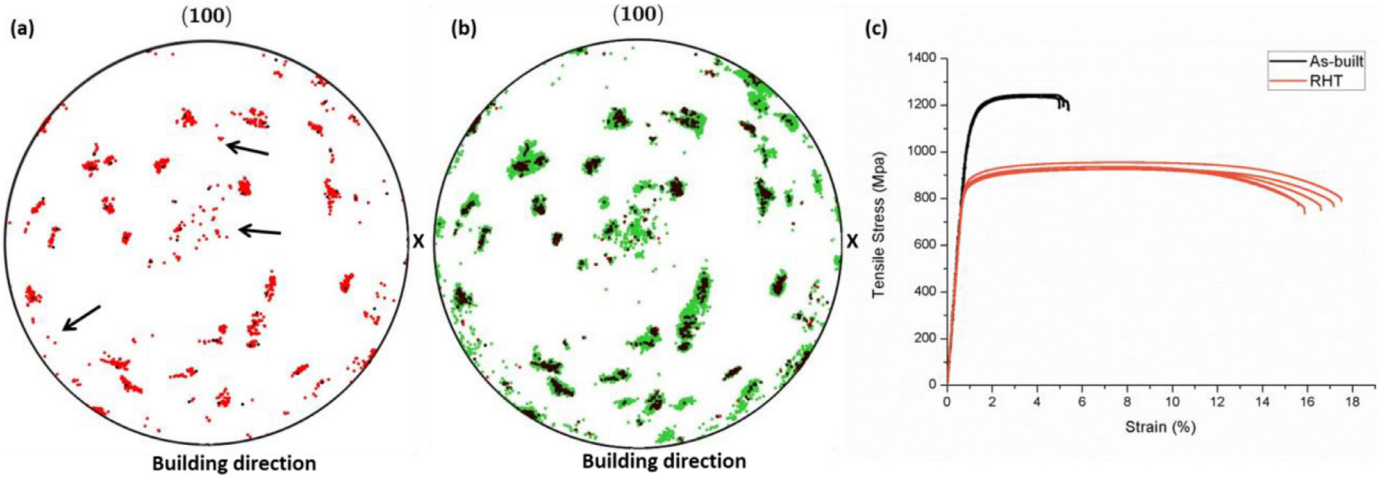

Fig. 4. (a) Overlaid discrete pole figures of calculated parent β (black) and measured β at 925 °C (red); (b) Overlaid discrete pole figures of measured β at 850 °C (green) and at 925 °C (red/black). (c) Engineering tensile stress-strain curves of Ti–6Al–4V specimens in the as-built condition and after RHT. (For interpretation of the references to color in this figure legend, the reader is referred to the web version of this article.)

formation occurs during the applied RHT. It is well understood however that RHT can retain the substructure of the martensitic phase to higher temperatures and promote higher nucleation rates of HAB grains [9]. This would exacerbate epitaxial recrystallization and result in observed significant refinement of the structure.

Fig. 3a shows the β-orientation map obtained by reconstructing the parent phase (β_1) of the room temperature α' phase. In Fig. 3b and c it is shown the measured β-orientation maps of the same location at 850° and 925 °C, respectively. The comparison of these maps allows the identification of the recrystallized β grains (some are marked in the corresponding figures via white arrows). As the temperature is increased from 850° to 925 °C, it is observed that the recrystallized β grains grow competitively with the surrounding matrix (β_1) and that some of the newly formed grains grow faster than others. In addition, these grains grow with no preferred grain growth direction aligned to any of sample coordinate system (as the heating is uniform as opposed to L-PBF). The retained α laths pin the original prior-β grain boundaries and therefore the overall β morphology remains unchanged during heat treatments below the β transus temperature. Subsequently, as the RHT was carried out above the β transus temperature no α-pinning could take place. It is plausible that the HAB, of higher mobility than the surrounding matrix β_1, could migrate at a higher rate [11] and thus change the original columnar morphology.

To examine the possible evolution of the texture during RHT, the pole figures of the as-built β are compared to those measured for a range of temperatures below the β transus (Fig. 4). Above the β transus temperature, abnormal grain growth occurs so it was not possible to directly observe changes in texture via EBSD. Below the β transus temperature, the dominant texture is that of the parent β phase (recrystallization during slow EBSD heating below the β transus temperature is limited). Minor texture components derived from the epitaxial recrystallization could only be identified through discrete pole figures. In Fig. 4a the reflections of the calculated β phase (referred to as β_1, i.e. the parent phase of the martensitic α' observed at room temperature) and those of the measured β at 925 °C are overlaid. It is observed that all the parent β orientations that present in the pole figures measured at 925 °C are within an orientation scatter of 10°. As β_1 does not show a large spread in orientation along the vertical axis of the columnar grain, it is unlikely that this possesses boundaries with high mobility capable of causing the refinement observed after RHT. On the other hand, the HAB recrystallized grains can be clearly observed as extra reflections at 925 °C and marked in the figure (arrows). By overlaying the reflections of the β phase measured at 850° and 925 °C (Fig. 4b) insights on the growth of the β phase can be evinced. It is noted that as the temperature increases from 850° to 925 °C, there is an apparent decrease in the orientation scatter due to the fact that each reflection describes the average orientation of several β sub-grains that are merging together. No further new β orientations appear during the growth of β phase from 850° to 925 °C as no additional HAB reflections are observed in Fig. 4b. This

Table 3
Tensile properties of Ti-6Al-4V produced under optimised conditions by L-PBF. The presented values are average and standard deviations from the 3 references. Specimens are built with consistent zx-orientation.

Condition	Young's modulus E (GPa)	Ultimate Tensile Strength UTS (MPa)	Yield Strength σ_y (Mpa)	Elongation ε (%)
As-built	124.3 ± 1.0	1241.6 ± 4.7	1122.9 ± 6.0	5.2 ± 0.2
Stress relieved (700 °C – 800 °C) [12-14]	106.5 ± 18.7	1036 ± 59.4	962 ± 62.1	11.0 ± 1.8
ASTM F2924-14 (900 – 950 °C) [6,12,15,16]	115.5 ± 2.4	1047.3 ± 138.9	982 ± 121.9	13.1 ± 0.8
RHTed (this study)	121.2 ± 0.8	934.5 ± 11.3	853.8 ± 10.7	16.6 ± 0.7

implies that most likely β_3 is not formed with random orientations to the surrounding phases but with BOR with α laths underneath the plane of observation.

The mechanical properties associated with the developed microstructure after RHT were assessed by comparing engineering stress-strain curves of the specimens before and after treatment (Fig. 4c). The specimens in the as-built condition showed high yield strength but limited elongation (5.2 ± 0.2%) which is not acceptable for typical industry standards (ASTM F3001/14). Following the RHT, a marked increase in elongation at break (16.6 ± 0.7%) and acceptable yield stress and UTS was observed. The difference in tensile properties is believed due to a combined effect of α coarsening (Supplementary Material, Fig. S1) and the β grain refinement. The balance in strength and ductility compares well to Ti–Al–4V produced by L-PBF followed by conventional post-processing heat treatments as well as to wrought and annealed products, as shown in Table 3, which suggests that the applied RHT is not penalising tensile properties although being conducted at temperatures above the β transus [2,4]. The proposed RHT method however brings significant advantages in terms of both process duration and refinement of the β structure alongside the consequent potential to generate specimens with isotropic behavior and increased fatigue resistance and fracture toughness.

To summarise, rapid heat treatments to a temperature in the single β phase region were carried on L-PBF Ti–6Al–4V specimens to investigate a methodology aimed at refining the columnar prior-β grains typical to AM. Fully laminar $\alpha+\beta$ microstructure with substantially refined prior-β grains could be obtained. The refinement is explained considering the epitaxial recrystallization that occurs at α/β interfaces from the substructure present in the as-built martensites. To-date, this has never been demonstrated in additively manufactured Ti alloys. High-temperature EBSD provides evidence of the early stages nucleation and growth of new HAB recrystallized β, which are believed to generate the refinement observed during RHT.

The present results would open a possibility for obtaining quasi-equiaxed microstructures following simple rapid heat treatments of AM specimens. The same methodology could be applied to refine the microstructure of a wider category of structural alloys in AM which display anisotropic behavior and limited fatigue resistance such as steels and Ni-based superalloys.

Declaration of Competing Interest

The authors declare that they have no known competing financial interests or personal relationships that could have appeared to influence the work reported in this paper.

Acknowledgments

The work presented here has been made possible by funding provided through the University of Nottingham's NanoPrime scheme and Ph.D. scholarship. Special thanks to Dr. Nigel Neate and Martin Roe (nano- and micro-scale Research Centre, University of Nottingham) for their support with the high-temperature EBSD experiments. Thanks to Dr. Ryan Maclachlan (Loughborough University) for his help with the EBSD investigations and the useful discussions.

Supplementary material

Supplementary material associated with this article can be found, in the online version, at doi:10.1016/j.scriptamat.2020.01.027.

References

[1] S. Balachandran, S. Kumar, D. Banerjee, On recrystallization of the α and β phases in titanium alloys, Acta Mater. 131 (2017) 423–434.
[2] X.-Y. Zhang, G. Fang, S. Leeflang, A.J. Böttger, A. Zadpoor, J. Zhou, Effect of subtransus heat treatment on the microstructure and mechanical properties of additively manufactured Ti-6Al-4V alloy, J. Alloys Compd. 735 (2018) 1562–1575.
[3] Y. Chong, T. Bhattacharjee, J. Yi, A. Shibata, N. Tsuji, Mechanical properties of fully martensite microstructure in Ti-6Al-4V alloy transformed from refined beta grains obtained by rapid heat treatment (RHT), Scr. Mater. 138 (2017) 66–70.
[4] Z. Zhao, J. Chen, H. Tan, G. Zhang, X. Lin, W. Huang, Achieving superior ductility for laser solid formed extra low interstitial Ti-6Al-4V titanium alloy through equiaxial alpha microstructure, Scr. Mater. 146 (2018) 187–191.
[5] R. Sabban, S. Bahl, K. Chatterjee, S. Suwas, Globularization using heat treatment in additively manufactured Ti-6Al-4V for high strength and toughness, Acta Mater. 162 (2019) 239–254.
[6] K. AmirMahyar, G. Ian, G. Moshe, L. Guy, On the role of different annealing heat treatments on mechanical properties and microstructure of selective laser melted and conventional wrought Ti-6Al-4V, Rapid Prototyp. J. 23 (2) (2017) 295–304.
[7] , ASTM E8/E8M-16a: Standard Test Methods for Tension Testing of Metallic Materials, ASTM International, West Conshohocken, PA, USA, 2016.
[8] M. Simonelli, Y.Y. Tse, C. Tuck, On the texture formation of selective laser melted Ti-6Al-4V, Metall. Mater. Trans. A 45 (6) (2014) 2863–2872.
[9] O.M. Ivasishin, R.V. Teliovich, Potential of rapid heat treatment of titanium alloys and steels, Mater. Sci. Eng.: A 263 (2) (1999) 142–154.
[10] A. Idhil Ismail, M. Dehmas, E. Aeby-Gautier, B. Appolaire, in: Proceedings of the 13th World Conference on Titanium, 2016, pp. 591–598.
[11] A.L. Pilchak, G.A. Sargent, S.L. Semiatin, Early stages of microstructure and texture evolution during beta annealing of Ti-6Al-4V, Metall. Mater. Trans. A 49 (2018) 908–919.
[12] B. Vrancken, L. Thijs, J.-P. Kruth, J. Van Humbeeck, Heat treatment of Ti6Al4V produced by selective laser melting: microstructure and mechanical properties, J. Alloys Compd. 541 (2012) 177–185.
[13] M. Simonelli, Y.Y. Tse, C. Tuck, Effect of the build orientation on the mechanical properties and fracture modes of SLM Ti–6Al–4V, Mater. Sci. Eng.: A 616 (2014) 1–11.
[14] Y. Xu, Y. Lu, K.L. Sundberg, J. Liang, R.D. Sisson, Effect of annealing treatments on the microstructure, mechanical properties and corrosion behavior of direct metal laser sintered Ti-6Al-4V, J. Mater. Eng. Perform. 26 (6) (2017) 2572–2582.
[15] Z. Fan, H. Feng, Study on selective laser melting and heat treatment of Ti-6Al-4V alloy, Results Phys. 10 (2018) 660–664.
[16] ASTM, ASTM F2924-14: Standard Specification for Additive Manufacturing Titanium-6 Aluminum-4 Vanadium with Powder Bed Fusion, ASTM International, 2014.